metals

MDPI

Article

Corrosion Behavior of API-X120 Carbon Steel Alloy in a GTL F-T Process Water Environment at Low COD Concentration

Dina Ewis [1], Ahmed Gomaa Talkhan [1], Abdelbaki Benamor [1,*], Hazim Qiblawey [2], Mustafa Nasser [1], Muneer M. Ba-Abbad [1] and Muftah El-Naas [1]

[1] Gas Processing Center, College of Engineering, Qatar University, P.O. Box 2713 Doha, Qatar; de1401951@student.qu.edu.qa (D.E.); a.gomaatalkhan@qu.edu.qa (A.G.T.); m.nasser@qu.edu.qa (M.N.); mbaabbad@qu.edu.qa (M.M.B.-A.); muftah@qu.edu.qa (M.E.-N.)

[2] Department of Chemical Engineering, College of Engineering, Qatar University, P.O. Box 2713 Doha, Qatar; hazim@qu.edu.qa

* Correspondence: benamor.abdelbaki@qu.edu.qa; Tel.: +974-4403-4381

Received: 8 March 2020; Accepted: 27 April 2020; Published: 27 May 2020

Abstract: The effect of temperature, time and rotation speed of FT-GTL process water on the corrosion rate of API X-120 carbon steel was investigated. Electrochemical impedance spectroscopy and potentiodynamic polarization techniques were used to determine the carbon steel corrosion rate under temperatures ranging from 293 to 323 K and rotation speed of 0, 500, 1000, 2000 rpm when the immersion time was 0.5, 1, and 2 h. The corrosion rate increased with temperature and rotation speed but decreased with immersion time. SEM, XRD, and XPS analyses of the corroded surfaces confirmed the formation of iron oxide and ferric oxide as the main components of the protective layer.

Keywords: corrosion; carbon steel API X120; GTL process water; electrochemical methods

1. Introduction

Energy sources play a fundamental role in the world's economics and the creation of wealth. Fossil fuels represent the biggest share in the world's energy mix and are expected to maintain this share in the near and medium-range future. Natural gas (NG) is becoming increasingly more important as a key energy component in the energy mix worldwide [1]. NG can be used for direct combustion for heat production as it can be used as a raw material in many synthesis gas process routes to be converted into a large number of liquid and gaseous products such as gas to liquid (GTL) products. In the GTL process, natural gas is converted through Fischer-Tropsch (FT) reactions into synthetic crude product that can be upgraded and separated into different commercial hydrocarbon fractions. A by-product of the FT reaction is the associated process wastewater that is generated in large volumes and may represent up to 25% more on a weight basis than the hydrocarbon products.

In a typical GTL plant, wastewater generally includes cooling tower blow down water, steam generation unit blow-down water and process area, equipment wash and maintenance activities in addition to FT reaction [2]. Table 1 shows wastewater sources and the main contaminants in each stream in a GTL process.

Table 1. Main sources of GTL wastewater

Unit	Contaminant
F-T reaction	Inorganic compounds and oxygenated hydrocarbons
Cooling tower blow down water	Dissolved solids, suspended solids and heavy metals
Steam generation unit blow-down water	Dissolved solids and minerals
Process area, equipment washing and maintenance activities	Oil, emulsified oil and other hydrocarbons

In particular, the characterization of FT reaction wastewater depends on the reaction conditions, such as the type of catalytic metal, temperature and pressure. GTL wastewater contains a number of inorganic compounds, including metals, chloride, sulphate, acetate, bicarbonate and dissolved gases such as H_2S and CO_2 [3]. Other contaminants in the water produced in the FT process include acidic contaminants and dissolved hydrocarbons such as acids, ketones, alcohol, aldehydes, acetates and other oxygenates that are mainly light alcohols which represent the main source of COD [4,5]. Detailed characterization of FT unit wastewater can be found in the work of Dang et al. [6].

Carbon steel material is commonly used in the fabrication of plant units and in pipelines transporting fluids in industrial processes for its economic advantages. The presence of acidic contaminants can corrode the internal surface of the pipeline network [7] and other plant units. Corrosion attacks on carbon steel represent real threats to the operations of the facilities, and for that reason, it is important to minimize the effect of corrosion on plant production and safety. Studies shows the microalloying of carbon steel with carbides and nitrides can reduce the corrosion rate and improve the mechanical properties and thus the price to yield ratio decreases [8]. API-X 70 and API-X80 were used in pipelines of oil and gas industry for their good mechanical properties [9]. However, API-X 120 with enhanced mechanical properties has replaced both metals [10]. API-X 120 steel is the highest grade of carbon steel pipeline that is available in today's market; it is developed and enhanced to resist the corrosion of pipelines even in sour environment [8].

In this work, we investigated the effect of temperature, immersion time and rotation speed of FT process wastewater that contains dissolved oxygenated hydrocarbons on the corrosion rate of API X-120 carbon steel using electrochemical methods.

2. Experimental Set-Up and Procedures

2.1. Material and Solution

2.1.1. Working Electrode

The working electrode consisted of an API X-120 carbon steel alloy rod having a diameter of 1.02 cm and an exposed surface area of approximately 0.823 cm^2. The working electrode was mounted on a resin sample holder and used in all experiments. Its elemental composition was taken from a previous work [8].

2.1.2. GTL Produced Water Characterization

The water sample was collected from a GTL plant in Qatar specifically from a F-T process unit. The water sample composition was analyzed and determined in our laboratory and is listed in Table 2. Mineral composition of the wastewater water sample was characterized by ICP-MS and is presented in Table 3.

Table 2. Analysis results of F-T process waste water.

Parameter, Dimension, (SMWW Method)	Value	Used Method
TOC, mg/L	125.4	Total organic carbon analyser (TOC-L)
COD, mg/L	530	APHA 5220 C Closed Reflux, Titrimetric Method
Phenols, mg/L	0.131	HAC spectrophotometer
PH, (4500 H+. B)	4.18	Electrometric Method
Conductivity, µs/cm	124.6	Conductivity meter
Salinity, ppt	0.06	Standard method
TDS, mg/L	38.5	Standard method
TSS, mg/L (APHA 2540 B)	2.5	Total Suspended Solids Dried at 103–105 °C

Table 3. Characterization of GTL produced water by IC-ICP-MS.

Component	Unit	Concentration
Ammonium	ppm	8.450
Potassium	ppm	0.058
Calcium	ppm	2.044
Magnesium	ppm	0.068
Boron	ppb	<dl *
Vanadium	ppb	0.018
Iron	ppb	31.144
Copper	ppb	0.314
Barium	ppb	<dl

* dl: detection limit.

2.2. Experimental Set-Up

Corrosion tests were performed in a classic three-electrode electrochemical double jacketed glass cell having a volume of 125 mL purchased from Gamry (Warminster, PA, USA). A 6 mm dimeter graphite counter electrode was mounted on the cell. The reference electrode employed in this work for electrochemical measurements consisted (Ag/AgCl) electrode filled with a KCl 3 molars solution emerged inside a Luggin capillary that was filled with GTL process water. The working electrode was immersed inside the solution and maintained at fixed temperature. The corrosion cell temperature was maintained at the desired temperature using a HAAKE A25 digital water circulator system (Thermo Scientific, Inchinnan, UK) that was connected to a double jacketed cell as shown in Figure 1. The solution concentration was maintained constant throughout the experimental runs by mounting a condenser on the cell opening to condense any evaporated solution during higher temperature experiments. The stirring speed of the solution was maintained at the lowest possible value to prevent any disturbance to the system while still ensuring good mixing at the same time.

A Gamry Ref 600 potentiostat (Gamry Instruments, inc. USA) with ±0.2% accuracy on potential and current readings was used for the electrochemical experiments. The potentiostat was controlled by Gamry GPES version 4.9.007 software. Recorded corrosion data were analyzed using Gamry Echem Analyst^{TM} Software [11,12]. Reproducibility of the experimental set up was verified in a previous work [7] and was estimated to be less than 6% error.

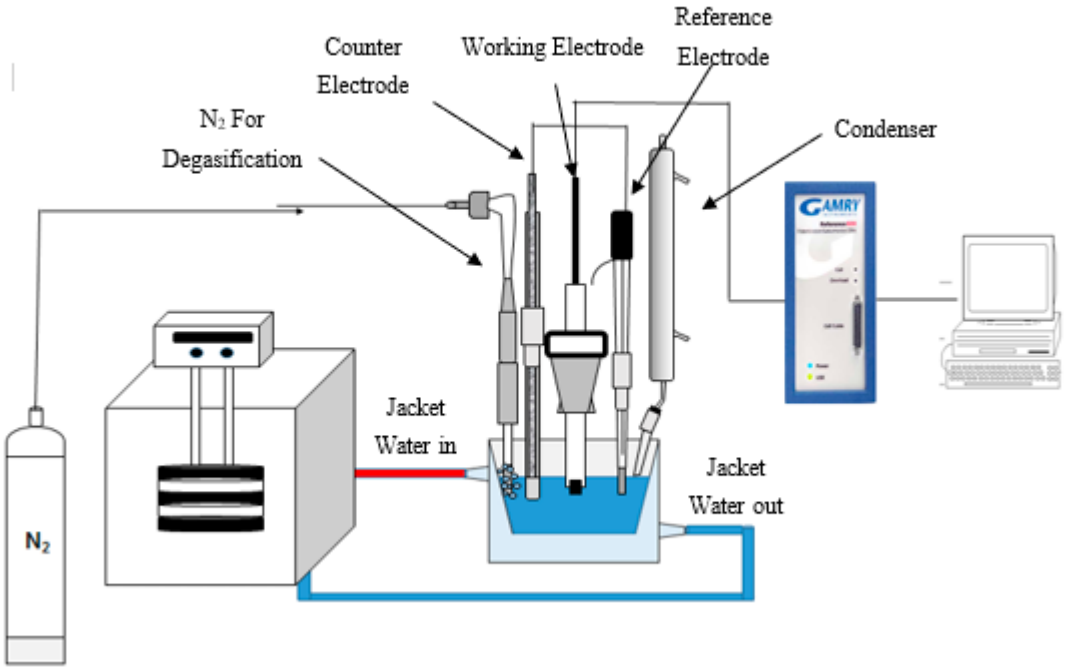

Figure 1. Schematic diagram of the experimental setup.

2.3. Electrochemical Measurement

The experimental work started with the preparation of the working rotating disc electrode that was first abraded with different grit papers (220, 400, 600, 800, 1000 and 2000) to remove all impurities and ensure a smooth surface, then it was successively cleaned with distilled water and acetone before letting it dry. Once the electrode was mounted on the cell, nitrogen gas was passed through the cell to deoxygenate its contents and remove any possible gas impurities in the cell. The open circuit potential (OCP) was measured before it reached stability defined as OCP <5 mV/20 min. During the EIS tests, signal frequencies varying from 0.001 Hz to 100 kHz were implemented. The applied disturbance signal was a sinusoidal voltage of 10 mV amplitude. The Tafel and linear polarization curves were carried out over a potential range of ±250 mV versus open circuit potential (OCP) with a scan rate of 1 mV/s. The solution temperatures were varied from 293 to 323 K in increment of 10 K. Working electrode rotation speeds of 0, 500, 1000, and 2000 (RPM) corresponding to a linear velocity of 0, 0.26, 0.53 and 1.06 m/s were applied. The specimen immersion times of 0, 30, 60 and 120 min were employed. Each test was repeated three times and the average value was considered. A summary of the experimental conditions is given in Table 4.

Table 4. Summary of the experimental conditions used in this work.

Temperature (K)	Immersion Time (min)	Rotation Speed (RPM)
293, 303, 313, and 323	0, 30, 60, and 120	0, 500, 1000, and 2000

2.4. Morphology and Composition Analysis

A high-resolution camera was employed to visually inspect the corrosion product on the surface of the specimen. A model JCM-6000 scanning electron microscope (SEM, Jeol Ltd, Tokyo, JAPAN) with a beam voltage of 20 kV was used to determine the specimen morphologies prior and post corrosion experiments. The specimen surface was analyzed using a model Miniflex II X-ray diffractometer (XRD, Rigaku, Tokyo, Japan) to determine possible corrosion products. An Ultra Axis X-ray photoelectron spectrometer (XPS, Kratos, Manchester, UK) was used also to quantitatively identify the content of the corroded samples and compare them with the XRD analyses results.

3. Results and Discussion

3.1. Effect of Temperature.

3.1.1. Potentiodynamic Polarization

To evaluate the temperature effect on the corrosion process for carbon steel in GTL process water, carbon steel alloy API-X120 was tested at four different temperatures of 293, 303, 313, and 323 K. Potentiodynamic polarization curves for carbon steel corrosion in FT-GTL process water were obtained applying a scan rate of 1 mV/s over a potential interval of ±250 mV versus open circuit potential (OCP) are presented in Figure 2.

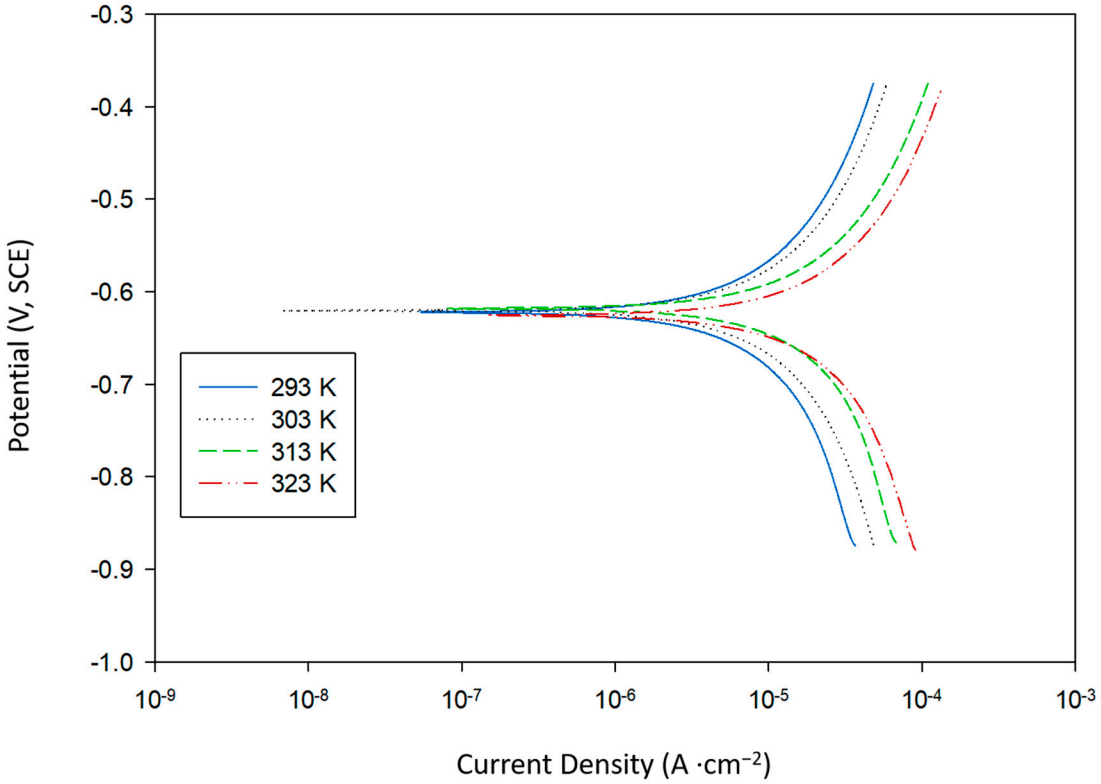

Figure 2. Potentiodynamic polarization curves for API X-120 steel alloy in GTL process water at different temperatures.

The obtained results showed that with increased solution temperature, Tafel curves shifted towards the right of the current density scale [13]. This shift in Tafel curves is attributed to the increased rate of metal dissolution which, in turn enhanced the oxidation-reduction reactions [14–18] as follows:

Oxidation reaction:

$$Fe_{(s)} \rightarrow Fe^{2+}{}_{(aq)} + 2e^{-} \quad (1)$$

The produced electrons from this reaction are used to reduce the oxygen dissolved in water according to the following reaction:

Reduction reaction:

$$O_{2\,(aq)}^{-} + 2H_2O_{(aq)} + 4e^{-} \rightarrow 4OH^{-} \quad (2)$$

Then the hydroxyl ions, OH^{-}, will undergo a chemical reaction with Fe^{2+} ions present in water to create iron hydroxide $Fe(OH)_2$, which eventually dries up to form ferric oxide (Fe_2O_3) [19] according to the following reaction:

$$Fe^{2+}{}_{(aq)} + 2OH^{-}{}_{(aq)} \rightarrow Fe(OH)_{2(aq)} \rightarrow Fe_2O_3 \ \ (rust) \quad (3)$$

The analysis of Tafel plots (Figure 2) allows the determination of electrochemical corrosion parameters such as the corrosion current density (i_{corr}), polarization resistance (R_p), and corrosion potential (E_{corr}) listed in Table 5. The cathodic Tafel slope (b_c) values were found to lay in the range 212–350 mV/decade, suggesting activation control corrosion. The analysis of Tafel plots using Echem Analyst™ allowed the determination of corrosion current (i_{corr}) which was used to calculate the corrosion rate, CR:

$$\mathrm{CR} = \frac{\left(1.95 \times 10^5\right) \cdot i_{corr} \cdot W}{\rho \cdot A} \tag{4}$$

where CR—corrosion rate-mille-inches/year (mpy), i_{corr} —corrosion current (Ampere), W—metal specimen equivalent mass (g), ρ—Metal density (g/cm^3) and A—contact area between the working electrode and the fluid (cm^2).

Stern–Geary equation [20] was used to determine the polarization resistance, R_p. The corrosion rate is determined by:

$$i_{corr} = \frac{(b_a \times b_c)}{(2.3 \times (b_a + b_c)} \cdot \frac{1}{R_p} \tag{5}$$

where the parameters (b_a) and (b_c) were determined from the anodic and cathodic Tafel slopes.

Table 5. Potentiodynamic polarization parameters for API-X120 steel in GTL process water at different temperatures.

Temperature (K)	293	303	313	323
Beta A (b_a), (V·decade^{-1})	0.189	0.24	0.222	0.270
Beta C (b_c), (V·decade^{-1})	0.212	0.280	0.290	0.350
R_p, [KΩ·cm^2]	5.691	4.619	2.562	2.256
Corrosion Current, *Icorr* (μA)	7.623	12.15	21.31	29.34
Corrosion Current Density (μA·cm^{-2})	9.26	14.76	25.89	35.65
Corrosion Potential, *Ecorr* (mV)	−621.8	−620.5	−618.3	−625.1
Corrosion rate (mpy)	4.238	6.753	11.85	16.31

It is worth noticing that as the temperature was increased from 293 to 323 K, a remarkable increase (up to nearly four-fold) in the corrosion rate was observed. According to NACE RP0775-2005 standard the corrosion rate is identified as high under the temperatures 293 and 303 K (5–10 mpy) and severe under the temperatures 313 and 323 K as the corrosion rate (mpy) is larger than 10. The increase in metal dissolution with increased temperature enhanced the oxidation-reduction reaction as well as the current density which are thought to be responsible for such behavior. The temperature effect on the process follows the well-known Arrhenius equation:

$$i_{\mathrm{corr}} = A \cdot \exp(-E_a / \mathrm{R}T) \tag{6}$$

where: A—a pre-exponential factor, E_a—apparent activation energy, R—gas constant (8.314 J·mol^{-1}·K^{-1}) and T—absolute temperature (K).

The Arrhenius plot in the form of log i_{corr} vs. $1/T$ for carbon steel alloy in GTL process water is shown in Figure 3. The plot gives a satisfactory straight line (R^2 = 0.9928) with a slope E_a/R = 4364.3. From this slope, the activation energy of carbon steel corrosion in the solution was estimated to be around 36.28 kJ/mol.

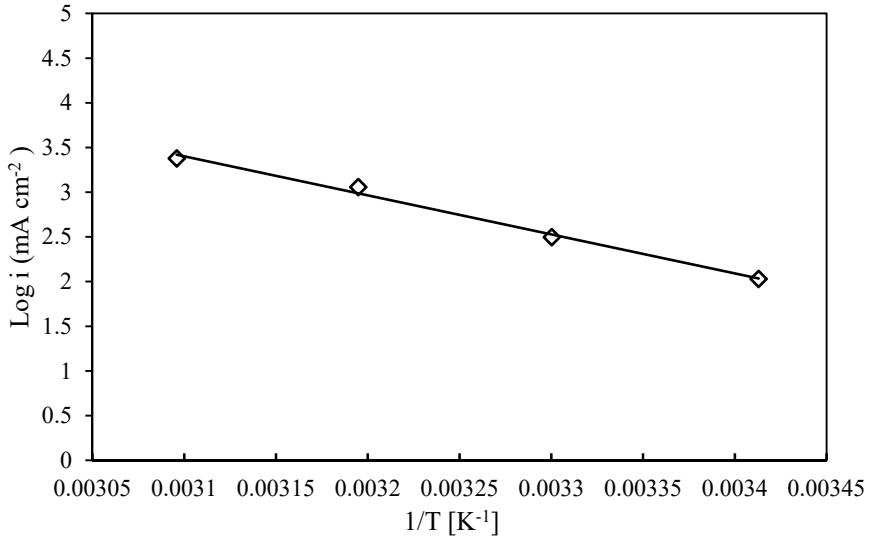

Figure 3. Arrhenius plots for the corrosion current of carbon steel in GTL process water solution.

3.1.2. Electrochemical Impedance Spectroscopy (EIS) Data Analysis

Electrochemical impedance spectroscopy (EIS) is an important tool to study corrosion and corrosion prevention. To further characterize the electrochemical corrosion process at the interface of API-X120 GTL-Process water environment, and to verify the results obtained by Tafel plots measurements, (EIS) measurements were performed. In this study, the equilibrium of the corrosion system was perturbed by applying a sinusoidal potential signal with an amplitude equals 10 mV across a frequency range from 100 mHz to 100 kHz at stabilized OCP. The response of system's current intensity against time changes for different solution temperatures was recorded. The Bode magnitude plot displays the log |Z| (log impedance modulus) versus log f (log frequency), and the Bode phase plot shows Φ (the phase angle) versus log f, where |Z| and Φ are defined as:

$$|Z| = [(Z')^2 + (Z'')^2]^{1/2} \quad (7)$$

and:

$$\Phi = \tan^{-1}[-Z''/Z'] \quad (8)$$

where Z′ and Z″ are the real and the imaginary components of the impedance, respectively.

The measured frequency characteristics of API-X120 steel alloy in corrosive environment of GTL process water at different temperatures are presented as Nyquist plots (Figure 4) and Bode plots (Figure 5) respectively. The EIS data on the Nyquist plot (Figure 4) shows a single semicircular loop in the first quadrant whose diameter increases with decreased temperature, which indicates a decrease in the corrosion rate of carbon steel. Nyquist plots show characteristic shapes of semi-circles suggesting that the corrosion process is under activation control. Larger diameter of the semicircles obtained with lower temperatures show high electrical resistance at the interface metal-solution, which is the result of oxidation of iron and Fe^{+2} ions in the solution. The EIS spectrum at different temperatures show the presence of one-time constant that is the capacitive loop. The presence of a capacitive loop, usually indicates that the sample surface was partially covered with corrosion products. The EIS diagrams at 293, 303, 313, and 323 K appeared to be identical in shape with a capacitive loop diameter which decreases with temperature. This results are in good agreement with those previously reported by other researchers [21,22].

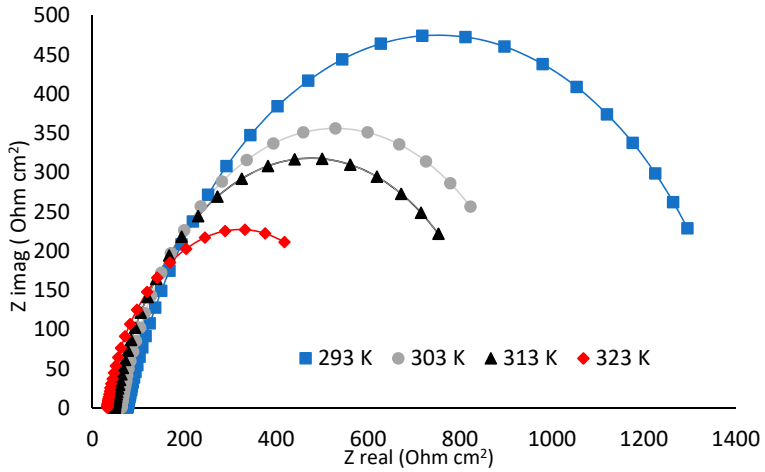

Figure 4. Nyquist diagrams for API-X120 steel in GTL process water solution determined experimentally (point line) and fitted ones (solid lines) at different temperatures.

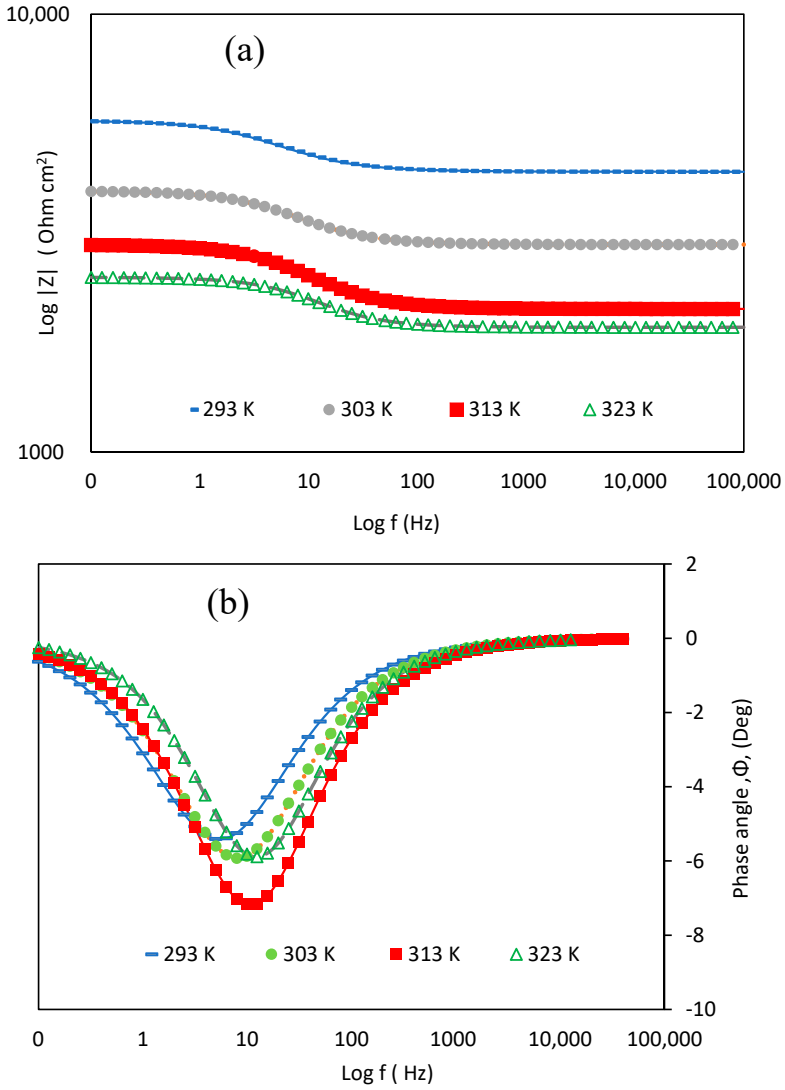

Figure 5. Bode curves of (**a**) phase angle vs frequency, and (**b**) modulus vs frequency. for API X-120 steel alloy in GTL process water solution experimentally (point line) and fitted (solid lines) at different temperatures.

The impedance spectra on the Bode plot (Figure 5) shows resistive regions at both ends of the frequency scale that are high (HF) and low (LF) frequencies. While at middle frequencies (MF), a capacitive behaviour was observed. The decrease in solution temperature increases the impedance absolute value (|Z|) at the LF, with the highest value obtained at a temperature of 293 K. On the other side, the larger value of the impedance |Z| at the low frequency (LF) range with decreased temperature is a criterion in favour that the corrosion resistance of carbon steel increases with temperature as a result of increased metal dissolution with temperature. The phase angle shift (Φ), revealed the presence of a single phase minimum (Φ_{min}) at the medium frequency range (MF), indicating the presence of one-time constant representing the electrode process. A lowest value for Φ_{min} was obtained at 313 K.

EIS data at different temperatures were analyzed with the Echem Analyst software using the equivalent circuit presented in Figure 6. This circuit is called the simplified Randles circuit. It consists of two resistances and a capacitor. Randles model is usually represented by a solution resistance (R_s) in series with a combination of a resistor (R_{ct}) and capacitor (C_{dl}) in parallel as shown in Figure 6. R_S represents the resistance of solution which is the GTL process water in this case. R_{ct} is the charge transfer resistance, it is the resistance for the electron to change the phase, e.g., from the electrode into the solution or to be more precise to a species solved in the solution. In order to get perfect fit, the substitution of constant phase elements (CPE) is correlated by the double-layer capacitance (Q_{dl} or C_{dl}) [21–24]. The resistor and capacitor usually represent the corrosion products formed on top of the sample surface. The transfer function used in the EC fitting is the following:

$$Z(w) = R_s + \frac{R_{ct}}{1 + (jw)^{\alpha} R_{ct} C_{dl}} \quad (9)$$

where: A—empirical parameter ($1 \leq \alpha \leq 1$), J—$\sqrt{-1}$, Ω—angular frequency ($\omega = 2\pi f$) in rad s^{-1} and F—frequency in Hz.

The value of the exponent alpha (α) in Equation (9) varies with the electrode surface roughness, smaller values of α indicate rougher surfaces [23]. When α is equal to unity, the system capacitance behaves as an ideal double-layer. Fitting values of the circuit show that both R_s and R_{ct} decrease with increased temperature with their lowest values obtained at the highest temperature (323 K), hence indicating increased corrosion rate with increased temperature [7,13,17,25]. These results obtained from EIS analyses confirmed the results previously obtained from the Tafel curves. The simulated electrical circuit parameters for carbon steel corrosion in GTL process water are summarized in Table 6.

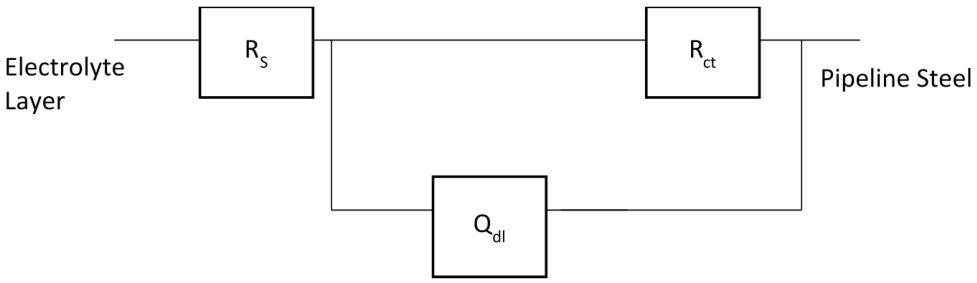

Figure 6. The electrochemical equivalent circuit used to fit EIS data for API-X120 steel in GTL process water at OCP with frequency.

Table 6. Fitting values to EIS at different temperatures.

Temperature (K)	R_s	R_{ct}	Q_{dl}	
			CPE	n-CPE
	[Ω·cm^2]	[Ω·cm^2]	[Ω^{-1}·cm^{-2} ·s^{-n}]	
293	76	1126	5.41×10^{-5}	0.78
303	63	723	5.95×10^{-5}	0.733
313	48	653	5.10×10^{-5}	0.784
323	32	412	6.53×10^{-5}	0.78

3.2. Effect of Immersion Time

The effect of specimen immersion time in GTL process water on carbon steel alloy API-X120 corrosion was evaluated at four different immersion times; 0, 30, 60 and 120 min at a fixed temperature of 303 K and zero rpm. Electrochemical measurements in term of Tafel curves and electrochemical impedance spectroscopy plots were used in the evaluation.

3.2.1. Potentiodynamic Polarization Curves

The obtained polarization curves for the tests conducted at different immersion times are presented in Figure 7.

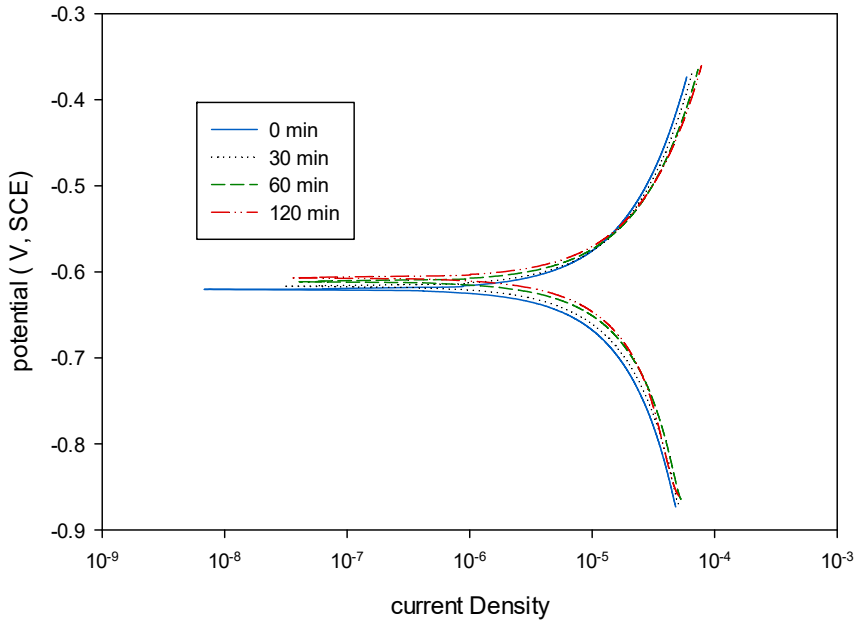

Figure 7. Potentiodynamic polarization curves of carbon steel alloy API-X120 in GTL process water at different immersion times.

Increasing the metal immersion time in the process water solution from 0 min to 120 min at a fixed temperature and zero rotational speed decreased the corrosion rate to reach a minimum rate of 5.28 mpy. This clearly indicates that the corrosion rate is greatly affected by the accumulation of the corrosion products on the surface of the metals which acts as a passive film against corrosion, the corrosion rate decreases. As this passive film layer thickness increases with time, the corrosion rate continues to decrease further. Numerical results obtained from the analysis of Tafel plots are summarized in Table 7.

Table 7. Effect of immersion time on corrosion rate of API-X120 in GTL water at 303 K.

Time (min)	0	30	60	120
Beta A (b_a), (V·decade^{-1})	0.240	0.205	0.177	0.145
Beta C (b_c), (V·decade^{-1})	0.280	0.214	0.187	0.154
R_p, [KΩ·cm^2]	4.619	4.155	3.841	3.414
Corrosion Current, Icorr (μA)	12.15	10.94	10.28	9.498
Corrosion Current Density (μA·cm^{-2})	14.76	13.29	12.49	11.54
Corrosion Potential, Ecorr (mV)	−620.5	−616.8	−611.7	−607.1
Corrosion rate (mpy)	6.753	6.083	5.715	5.28

3.2.2. Electrochemical Impedance Spectroscopy (EIS)

EIS curves at the different immersion times provide a clear indication on the corrosion rate. Nyquist and Bode plots show the effect of time interval from 0 to 120 min presented in Figures 8 and 9, respectively. Experimental EIS data were analyzed by the Echem-Analyst software using the equivalent circuit shown in Figure 6. The choice of the equivalent circuit was based on the comprehension of the normal and pitting corrosion as appeared in the visual and SEM observations presented in Sections 3.4.1 and 3.4.2 A good agreement exists between the experimental and simulated data shown in Nyquist plots (Figure 8) and Bode plots (Figure 9). Nyquist plot present a single semicircle loop in the first quadrant whose diameter increases with increased immersion time. The shape of semi-circles indicates the activation process control during corrosive material tests. The diameter of the capacitive loop increased with increasing the time interval, reaching the maximum diameter at 120 min which means that resistance to corrosion was maximum at 120 min [26].

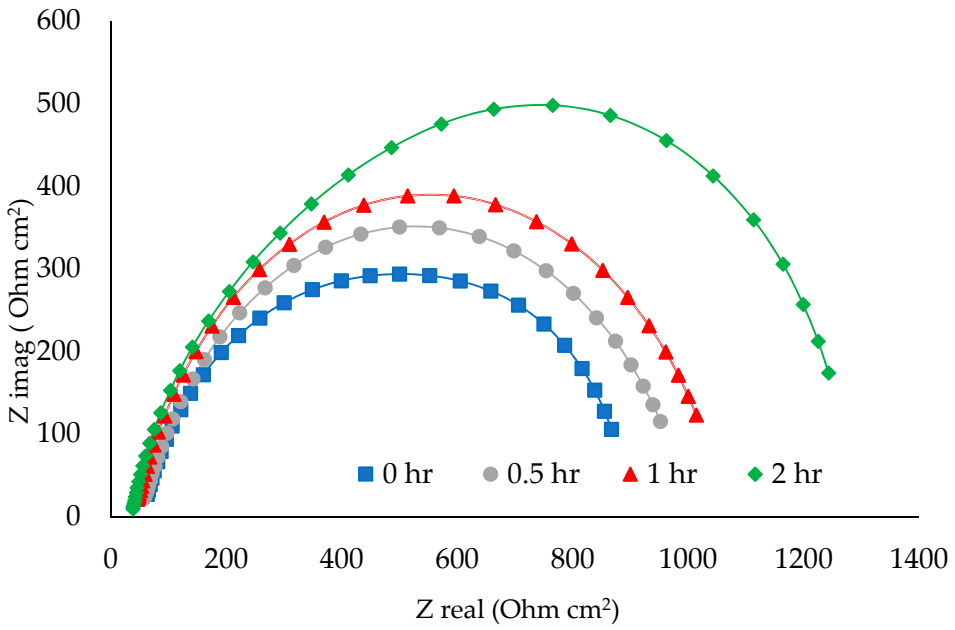

Figure 8. Nyquist plots for API X-120 steel alloy in GTL process water at different immersion times determined experimentally (point line) and fitted ones (solid lines).

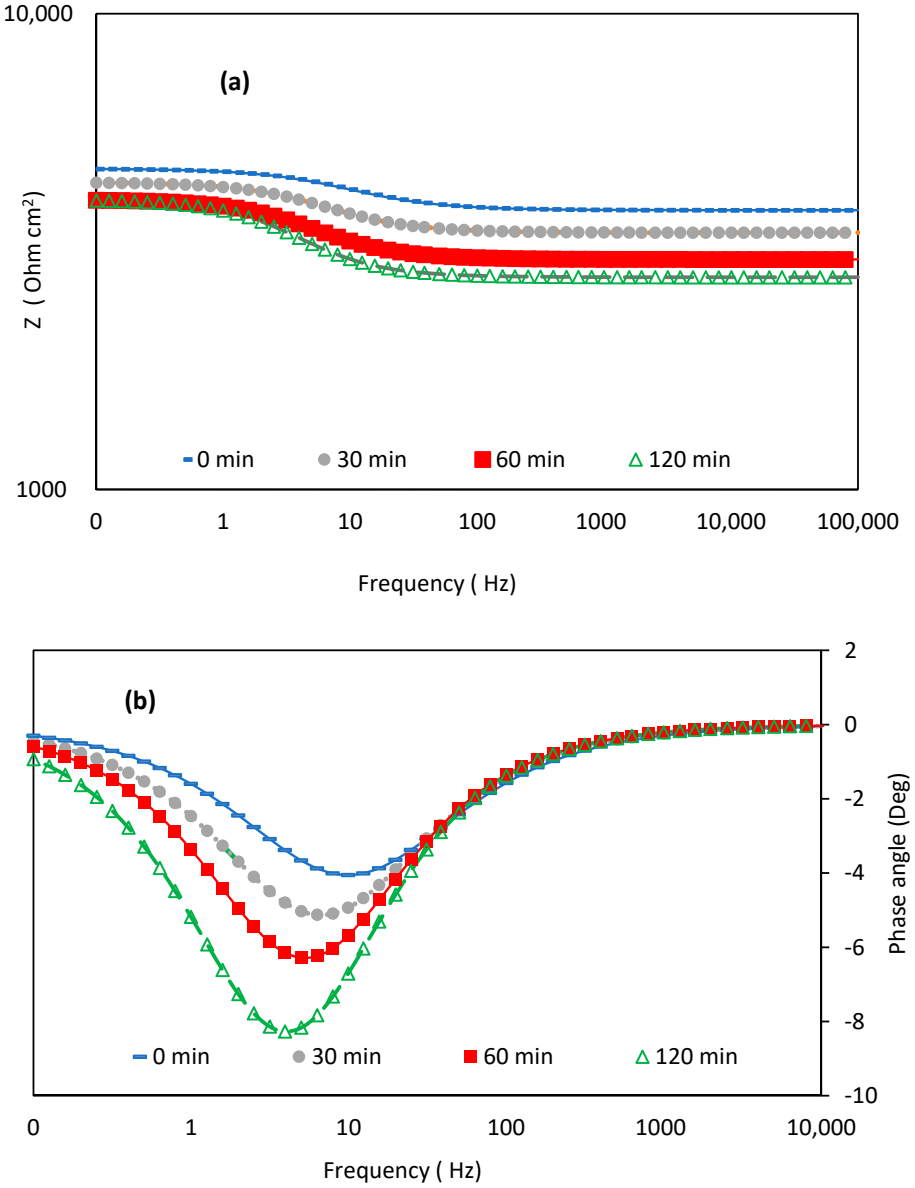

Figure 9. Bode plots of (**a**) phase angle vs frequency, and (**b**) modulus vs frequency. for API X-120 steel alloy in GTL process water at different immersion times.

The EIS spectrum at different immersion times showed the presence of a one time constant that is the capacitive loop usually attributed to adsorbed species on the metal surface [27], indicating the partial coverage of the metal surface with corrosion products. The characteristics of this capacitive loop are shown better in the bode plot. Figure 9b shows a clear shift in the phase. The bode plot just shows below 10 degrees of the phase angle, indicating that the capacitance characteristic is weak. This was predicted because the studied time is just two hours, it might become stronger by the time and the corrosion product would play the role of a barrier against corrosion.

The impedance spectra in the Bode format (Figure 9) show the presence of three different regions: a resistive region on the left side of the frequency axis representing high frequencies (HF) region, and low frequencies (LF) region on the right side of the axis. In the middle frequencies region (MF) a capacitive behaviour region was observed. The EIS data were fitted to the equivalent circuit shown in Figure 6 and obtained fitting values are presented in Table 8. The solution resistance (R_S) decreases with increasing immersion time, which can be understood by the fact that dissolved metal concentration increases with time making the solution more active and conductive to the current. On the other hand,

R_{ct} increases with time to reach a maximum value obtained at the immersion time of 120 min. This increase in R_{ct} can be explained that the increase in time led to the formation of a corrosion products layer that get thicker as time increases. The increase in the immersion time caused an increase in the total impedance (|Z|) at low frequency (LF) region with the highest value obtained for immersion time of 120 min as in Figure 9a. The total impedance usually refers to corrosion resistance so the diameter of the Nyquist plot has to be smaller when comparing the immersion time between 0 and 120 min. Whereas, the alloy corrosion resistance is determined by the parameter R_{ct} which is inversely proportional to corrosion current density [28]. Thus, increasing the value of the R_{ct} decrease the rate of corrosion. The phase angle shift (Φ) shown in Figure 9b indicates that a single phase minimum (Φ_{min}) at medium frequencies region (MF) suggesting the presence of only one time constant. Φ_{min} becomes lower over time, and the lowest value was recorded at 120 min. This denotes to a decrease in the medium frequency. This is also suggested a very stable film formation on the surface of the sintered alloy. Therefore, the experimental outcomes from EIS (Nyquist and Bode) results are in agreement with the potentiodynamic polarization results.

Table 8. Fitting results for EIS at different time.

Time (min)	R_s	R_{ct}	Q_{dl}	
			CPE	n-CPE
	$[\Omega \cdot cm^2]$	$[\Omega \cdot cm^2]$	$[\Omega^{-1} \cdot cm^{-2} \cdot s^{-n}]$	
0	63	723	5.95×10^{-5}	0.733
30	57	854	6.24×10^{-5}	0.787
60	44	904	6.74×10^{-5}	0.805
120	38	1204	6.73×10^{-5}	0.822

3.3. Effect of Rotation Speed

The effect of working electrode rotation speed on the API-X120 steel alloy in GTL process water was investigated at four different rotation speeds (0, 500, 1000, and 2000 rpm) and a fixed temperature of 293 K. The polarization curves obtained under these conditions, shown in Figure 10, indicate that the corrosion behavior of carbon steel is affected by the solution velocity (rotation speed).

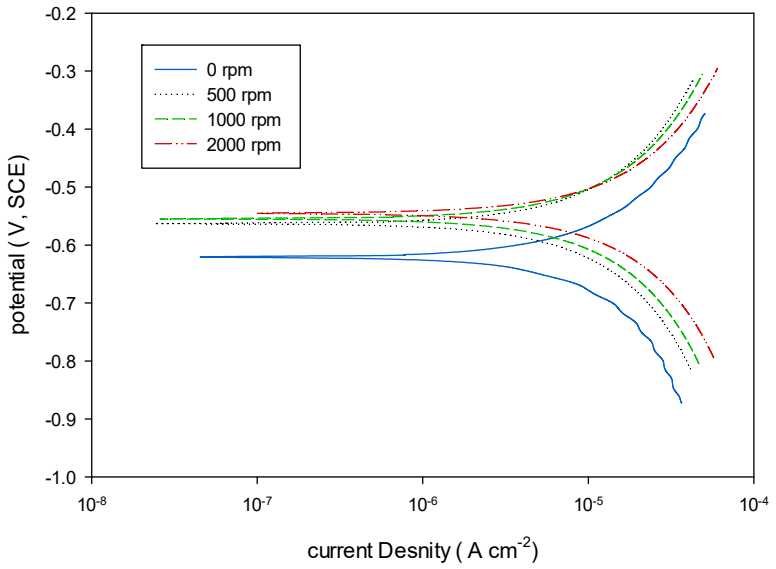

Figure 10. Potentiodynamic polarization curves for API X-120 steel alloy in GTL process water at different solution flowrates.

For static condition (0 rpm), the polarization curve shows an E_{corr} value around −621.8 mV and an i_{corr} value about 7.623 µA. As soon as the rotation speed increased, the E_{corr} value shifted to a higher value of −563 mV at 500 rpm. The E_{corr} value increased slightly at 1000 rpm for a value of −555 mV followed by a further slight increase for a rotation speed of 2000 rpm to reach a value of −545 mV. The i_{corr} value increased also with the increase in the rotation speed, reaching the highest value at of 10.83 µA at 2000 rpm which is similar to what was reported by Lopes et al. [29]. A summary of the results is presented in Table 9.

Table 9. The effect of rotation speed on corrosion rate at 293 K.

Speed (rpm)	0	500	1000	2000
Beta A (b_a), (V·decade^{-1})	0.189	0.222	0.226	0.207
Beta C (b_c), (V·decade^{-1})	0.212	0.223	0.224	0.218
R_p, [KΩ·cm^2]	5.691	5.943	5.24	4.255
Corrosion Current, *Icorr* (µA)	7.623	8.128	9.322	10.83
Corrosion Current Density (µA·cm^{-2})	9.26	9.88	11.33	13.16
Corrosion Potential, *Ecorr* (mV)	−621.8	−563	−555	−545
Corrosion rate (mpy)	4.238	7.747	8.885	10.33

The analysis of the Tafel plots (Figure 10) suggests that increased solution velocity (rotation speed) generated high current densities which caused a significant reduction in the oxidizing agents' concentration in the solution. Beside this, mass transport from and to the corroding metal may have been enhanced by increased rotation speed. The observed relatively constant cathodic and anodic Tafel slopes under dynamic conditions, suggest the presence of a uniform mechanism for iron dissolution and cathodic reduction reactions. The induced turbulent environment with increased rotation speed caused a deterioration of formed layer which caused an increase in the corrosion rate [7,30–32].

3.4. Morphology Analysis

3.4.1. Visual Observation

Visual observation of three carbon steel alloy specimens was performed using a digital camera. The obtained pictures are shown in Figure 11.

(**a**) (**b**) (**c**)

Figure 11. Visual images of blank and corroded surfaces of specimens, (**a**) Blank carbon steel specimen, (**b**) Carbon steel In GTL water at 0 rpm and 323 K, (**c**) Carbon steel In GTL water at 1000 rpm and 298 K.

The carbon steel specimens were blank carbon steel alloy, carbon steel alloy exposed to GTL water at 323 K and zero rotation speed while third specimen was exposed to GTL water at 1000 rpm and 298 K. both specimens were exposed to the corrosive environment for 24 h. It was observed that carbon steel alloy exposed to a temperature of 323 K has dark spots and gravures that result from pitting corrosion, while the specimen that was exposed to GTL water at 1000 rpm and 298 K has a sallow layer. Of course, the blank specimen does not show any visual defect nor marks.

3.4.2. Scanning Electron Microscope (SEM) Analysis

Blank and corroded carbon steel alloys were analysed using a scanning electron microscope. The specimens were exposed to the same conditions described in Section 3.4.1. The obtained images, shown in Figure 12, reveal that blank condition carbon steel alloy has only a few scratches caused by the grit paper during the specimen cleaning process, similar to what was visually observed earlier without any serious surface damage. Comparing the blank surface specimen, the corroded surface at 323 K and zero rotation speed shows pitting corrosion that was also clear by visual observation. SEM for the corroded surface at 1000 rpm and 323 K shows the formation of a shallow corrosion product layer. These corrosion products in both cases are mainly iron oxide.

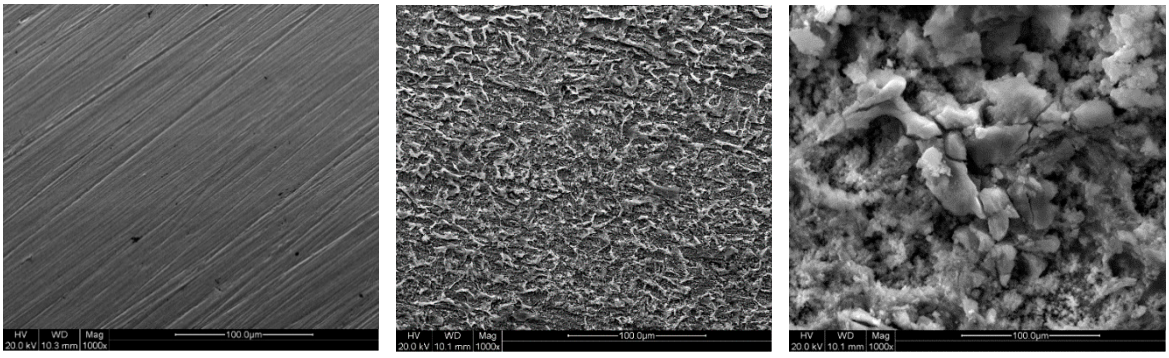

(**a**) (**b**) (**c**)

Figure 12. Scanning electron microscope (SEM) images of (**a**) blank and corroded surfaces, (**b**) 323 K, (**c**) 1000 rpm.

3.5. XRD Analysis

The XRD spectra of the API-X-120 carbon steel corrosion products at 1000 rpm after 24 h are presented in Figure 13. The spectra revealed the presence of a high-intensity peak at 44.6° 2θ in the corroded specimen. This peak is attributed to the presence of (Fe) iron. Beside this, different peaks at low intensity 2θ attributed to the presence of Fe_2O_3 were found on the surface of corroded metal against a small unique peak for Fe_2O_3 found in the reference specimen. Trace amounts of Fe_2O_3 were also found in the blank specimen which may be attributed to the contaminations from the extern. The presence of iron oxide (III) (Fe_2O_3) as the main corrosion product. Indicates that H_2O is the main component causing corrosion according to Equations (1)–(3). The factors that accelerated the rate of corrosion could be temperature, chemical salts, humidity and pollutants presented in Table 1. Production of iron oxide-III (Fe_2O_3) is believed to form a layer on top of the steel specimen surface slowing down the corrosion rate. These results are in agreement with the findings reported by Kitamura et al. [33].

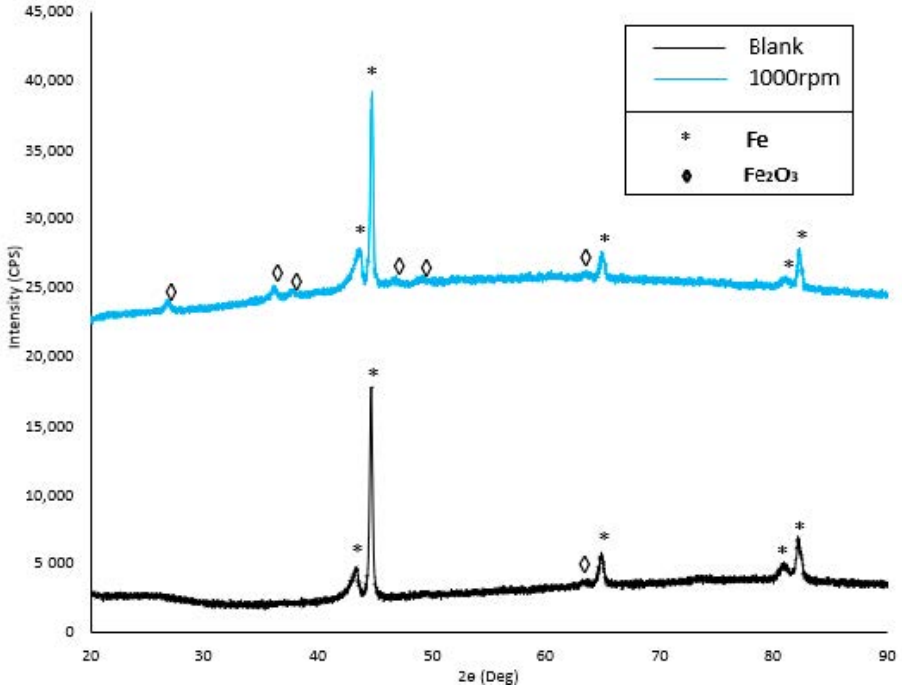

Figure 13. XRD fitting spectrum obtained from corrosion product layer at 1000 rpm after 24 h.

3.6. XPS Analysis

The composition of the corrosion product formed on API-X 120 carbon steel in GTL process water under the given conditions of 1000 rpm at ambient temperature was determined using XPS analysis. The XPS fitting curves and depth profiles are shown in Figure 14. The Figure show that the binding energies of iron, oxygen, and carbon were essentially the same. The peaks in the C1s spectra was obtained at 288.3 eV, O1s spectra at 531.5 eV while Fe2p spectrum were obtained at 710.6 eV and 723.4 eV respectively confirming the presence of amorphous Fe_2O_3. The XPS analysis results confirmed the results previously obtained by XRD analysis, as both showed the presence of amorphous Fe_2O_3 on the surface of corroded specimens.

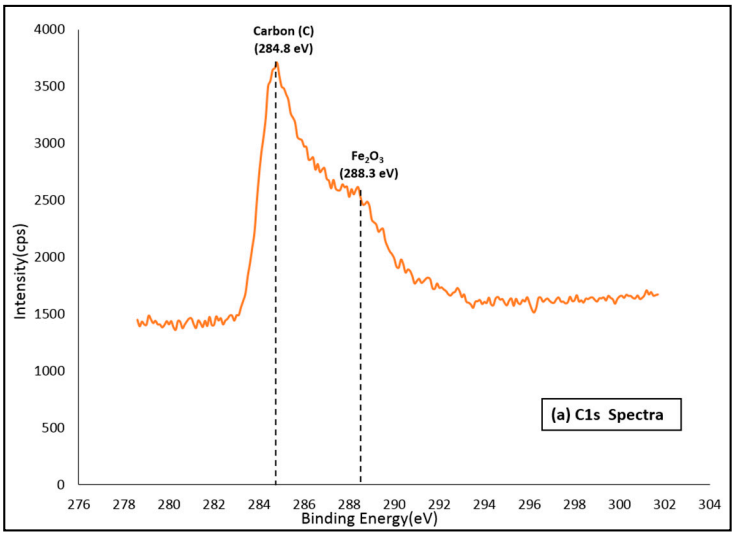

(**a**)

Figure 14. *Cont.*

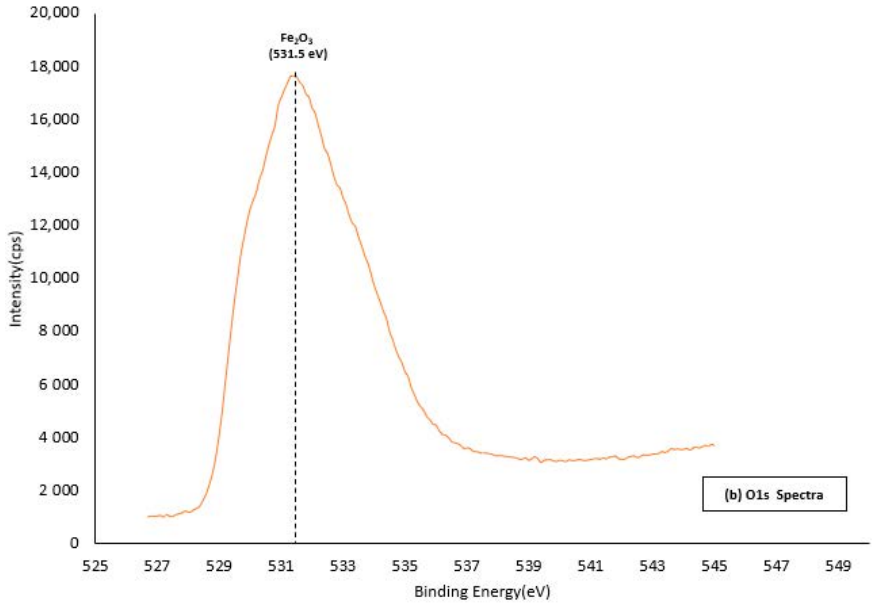

(**b**)

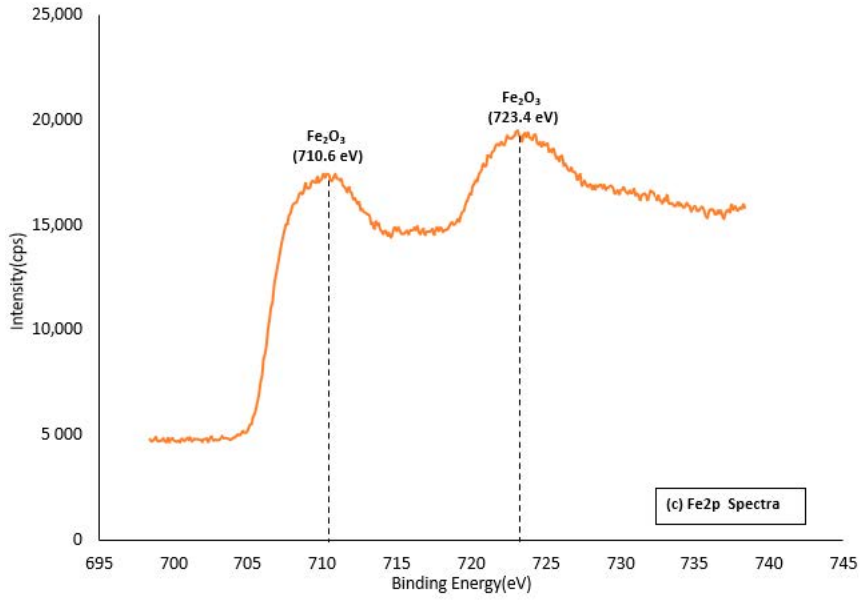

(**c**)

Figure 14. XPS fitting spectra obtained from corrosion product layer at 1000 rpm after 24 h. (**a**) C1s characteristic peak, (**b**) O1s characteristic peak, and (**c**) Fe2p characteristic peak.

Similar findings were reported by Sun et al. [34] who proved the presence of amorphous Fe_2O_3 during the initial stage of corrosion. The presence of trace amounts Fe_2O_3 on the blank specimen (before immersion in the corrosive solution) is normally attributed to surrounding contaminants.

4. Conclusions

In this work, the corrosion behavior and corrosion rate of API-X120 carbon steel alloy in GTL plant process water at different temperatures, rotational speeds and specimen immersion times was investigated using electrochemical techniques. It was found that the corrosion rate increased as the

solution temperature increased up to 16.31 mpy at 323 K. this was attributed to the metal dissolution, which in turn enhanced the oxidation-reduction reactions. Similar behavior was observed on the corrosion rate when the turbulence of the solution increased, where it caused a progressive removal of the protective layer on the specimen surface that led to an increase in the corrosion rate. An increase in the immersion time caused the corrosion rate to decrease a result of the formation of a homogenous passive film layer from the corrosion products on the specimen surface. Visual inspection and SEM micrographs reveled the existence of pitting and several cracks on the specimen surface. XRD confirmed the formation of amorphous iron oxide-III (Fe_2O_3) layer on the specimen surface, which was also confirmed by the XPS analysis.

Author Contributions: Conceptualization: A.B., H.Q.; Data curation: D.E., A.G.T., A.B.; Formal analysis: D.E., A.G.T., A.B., M.N., Funding acquisition: A.B., M.E.-N.; Investigation: D.E., A.G.T., M.M.B.-A.; Methodology: D.E., A.B., M.N., M.E.-N.; Project administration: D.E., A.B., M.E.-N.; Resources: H.Q., M.N., M.M.B.-A.; Software: D.E., A.B., M.E.-N.; Supervision: A.B., H.Q.; Validation: A.B., M.N., M.M.B.-A., M.E.-N.; Visualization: D.E., A.G.T., M.M.B.-A.; Writing - original draft: D.E., A.G.T.; Writing - review & editing: D.E., A.G.T., A.B. All authors have read and agreed to the published version of the manuscript.

Funding: This research was made possible by an NPRP Grant # 10-0127-170270 from the Qatar National Research Fund (a member of Qatar Foundation). The statements made herein are solely the responsibility of the authors.

Acknowledgments: The authors would like to acknowledge the technical support of CLU Qatar University in performing SEM images.

Conflicts of Interest: The authors declare no conflict of interest.

References

1. Sönmez, E.; Kekre, S.; Scheller-Wolf, A.; Secomandi, N. Strategic analysis of technology and capacity investments in the liquefied natural gas industry. *Eur. J. Oper. Res.* **2013**, *226*, 100–114. [CrossRef]
2. Neerkathalingam, P.S.; Van Vuuren, M.J. Process Wastewater Treatment and Management in Gas to Liquids Industries. In *SPE Oil and Gas India Conference and Exhibition*; Society of Petroleum Engineers: Richardson, TX, USA, 2010.
3. Onwusogh, U. Feasibility of Produced Water Treatment and Reuse—Case Study of a GTL Plant. In Proceedings of the International Petroleum Technology Conference 2015, Doha, Qatar, 6–9 December 2015.
4. Majone, M.; Aulenta, F.; Dionisi, D.; D'Addario, E.N.; Sbardellati, R.; Bolzonella, D.; Beccari, M. High-rate anaerobic treatment of Fischer–Tropsch wastewater in a packed-bed biofilm reactor. *Water Res.* **2010**, *44*, 2745–2752. [CrossRef] [PubMed]
5. Wang, D.; Han, H.; Han, Y.; Li, K.; Zhu, H. Enhanced treatment of Fischer-Tropsch (FT) wastewater using the up-flow anaerobic sludge blanket coupled with bioelectrochemical system: Effect of electric field. *Bioresour. Technol.* **2017**, *232*, 18–26. [CrossRef] [PubMed]
6. Wang, D.; Ma, W.; Han, H.; Li, K.; Hao, X. Enhanced treatment of Fischer–Tropsch (FT) wastewater by novel anaerobic biofilm system with scrap zero valent iron (SZVI) assisted. *Biochem. Eng. J.* **2017**, *117*, 66–76. [CrossRef]
7. Benamor, A.; Talkhan, A.G.; Nasser, M.; Hussein, I.; Okonkwo, P.C. Effect of temperature and fluid speed on the corrosion behavior of carbon steel pipeline in Qatari oilfield produced water. *J. Electroanal. Chem.* **2018**, *808*, 218–227. [CrossRef]
8. Bahgat Radwan, A.; Sliem, M.H.; Okonkwo, P.C.; Shibl, M.F.; Abdullah, A.M. Corrosion inhibition of API X120 steel in a highly aggressive medium using stearamidopropyl dimethylamine. *J. Mol. Liq.* **2017**, *236*, 220–231. [CrossRef]
9. Wang, X.; Song, X.; Chen, Y.; Wang, Z.; Zhang, L. Corrosion Behavior of X70 and X80 Pipeline Steels in Simulated Soil Solution. *Int. J. Electrochem. Sci.* **2018**, *13*, 6436–6450. [CrossRef]
10. Paul, S.; Pattanayak, A.; Guchhait, S.K. Corrosion behavior of carbon steel in synthetically produced oil field seawater. *Int. J. Metals* **2014**, 628505. [CrossRef]
11. Din Yati, M.S.; Derman, M.; Isa, M.; Muhammad, M.M.; Nain, H. Electrochemical Characterisation of Hybrid Activators for Aluminium Sacrificial Anodes in Natural Sea Water. *Def. S&T Tech. Bull.* **2013**, *6*.

12. Kugel, A.J.; Jarabek, L.E.; Daniels, J.W.; Vander Wal, L.J.; Ebert, S.M.; Jepperson, M.J.; Stafslien, S.J.; Pieper, R.J.; Webster, D.C.; Bahr, J. Combinatorial materials research applied to the development of new surface coatings XII: Novel, environmentally friendly antimicrobial coatings derived from biocide-functional acrylic polyols and isocyanates. *J. Coat. Technol. Res.* **2009**, *6*, 107–121. [CrossRef]
13. Desimone, M.P.; Gordillo, G.; Simison, S.N. The effect of temperature and concentration on the corrosion inhibition mechanism of an amphiphilic amido-amine in CO 2 saturated solution. *Corros. Sci.* **2011**, *53*, 4033–4043. [CrossRef]
14. Veawab, A.; Tontiwachwuthikul, P.; Chakma, A. Corrosion behavior of carbon steel in the CO_2 absorption process using aqueous amine solutions. *Ind. & Eng. Chem. Res.* **1999**, *38*, 3917–3924.
15. Zhao, B.; Sun, Y.; Yuan, Y.; Gao, J.; Wang, S.; Zhuo, Y.; Chen, C. Study on corrosion in CO_2 chemical absorption process using amine solution. *Energy Procedia* **2011**, *4*, 93–100. [CrossRef]
16. Porcayo-Calderon, J.; Escalera, L.M.; Canto, J.; Casales-Diaz, M.; Salinas-Bravo, V. Effect of the Temperature on the CO_2-Corrosion of Ni3Al. *Int. J. Electrochem. Sci.* **2015**, *10*, 3136–3151.
17. Gürten, A.A.; Keleş, H.; Bayol, E.; Kandemirli, F. The effect of temperature and concentration on the inhibition of acid corrosion of carbon steel by newly synthesized Schiff base. *J. Ind. Eng. Chem.* **2015**, *27*, 68–78. [CrossRef]
18. Esmaily, M.; Shahabi-Navid, M.; Svensson, J.-E.; Halvarsson, M.; Nyborg, L.; Cao, Y.; Johansson, L.-G. Influence of temperature on the atmospheric corrosion of the Mg–Al alloy AM50. *Corros. Sci.* **2015**, *90*, 420–433. [CrossRef]
19. Haile, T.; Sopkow, L.; Choi, L.; Wolodko, J.; Tsaprailis, H. Corrosivity of Produced and Make-up Water in Oil Sands Thermal Water Treatment Systems. In *NACE International Corrosion Conference Proceedings*; NACE International: Houston, TX, USA, 2016.
20. Stern, M.; Geaby, A.L. Electrochemical polarization I. A theoretical analysis of the shape of polarization curves. *J. Electrochem. Soc.* **1957**, *104*, 56–63. [CrossRef]
21. Melot, D.; Paugam, G.; Roche, M. Disbondments of pipeline coatings and their effects on corrosion risks. *J. Prot. Coat. Linings* **2009**. Available online: https://pdfs.semanticscholar.org/e96f/faa69e0368a901b19f319923b262fb8fcbae.pdf (accessed on 20 March 2020).
22. Wang, X.; Xu, J.; Sun, C.; Yan, M. Effect of oilfield produced water on corrosion of pipeline. *Int. J. Electrochem. Sci.* **2015**, *10*, 8656–8667.
23. Leibig, M.; Halsey, T.C. The double layer impedance as a probe of surface roughness. *Electrochim. Acta* **1993**, *38*, 1985–1988. [CrossRef]
24. Maocheng, Y.; Jin, X.; Libao, Y.U.; Tangqing, W.; Cheng, S.U.N.; Wei, K.E. EIS analysis on stress corrosion initiation of pipeline steel under disbonded coating in near-neutral pH simulated soil electrolyte. *Corros. Sci.* **2016**, *110*, 23–34. [CrossRef]
25. Harris, M. Effects of Corrosion Inhibitor on the Corrosion Behavior of Low Carbon Steel in CO_2 Environment. 2017. Available online: https://ideaexchange.uakron.edu/honors_research_projects/475/ (accessed on 8 March 2020).
26. Mustafa, C.M.; Rahman, A.K.M.O.; Begum, D.A. Effects of time and temperature on the mild steel corrosion inhibition by molybdate and nitrite. *Indian J. Chem. Technol.* **1996**, *3*, 44–48.
27. Keddam, M.; Mottos, O.R.; Takenouti, H. Reaction model for iron dissolution studied by electrode impedance I. Experimental results and reaction model. *J. Electrochem. Soc.* **1981**, *128*, 257–266. [CrossRef]
28. Baig, M.; Ammar, H.R.; Seikh, A.H.; Alam, M.A.; Alharthi, N.H. Effect of Immersion Time and Temperature on Corrosion Behaviour of Nanocrystalline Al-Fe-Cr Alloy. *J. Electrochem. Sci.* **2017**, *12*, 3336–3349. [CrossRef]
29. Lopes-Sesenes, R.; Dominguez-Patiño, G.F.; Gonzalez-Rodriguez, J.; Uruchurtu, J. Effect of flowing conditions on the corrosion inhibition of carbon steel by extract of buddleia perfoliata. *Int. J. Electrochem. Sci.* **2013**, *8*, 477–489.
30. Tian, J.; Huang, H.; Pan, Z.-Q.; Zhou, H. Effect of flow velocity on corrosion behavior of AZ91D magnesium alloy at elbow of loop system. *Trans. Nonferrous Metals Soc. China* **2016**, *26*, 2857–2867. [CrossRef]
31. Shen, S.; Yang, Y.-N.; Bian, Y.; Zhao, Y. Kinetics of CO_2 absorption into aqueous basic amino acid salt: Potassium salt of lysine solution. *Environ. Sci. & Technol.* **2016**, *50*, 2054–2063.
32. Ortega-Toledo, D.M.; Gonzalez-Rodriguez, J.G.; Casales, M.; Martinez, L.; Martinez-Villafañe, A. CO_2 corrosion inhibition of X-120 pipeline steel by a modified imidazoline under flow conditions. *Corros. Sci.* **2011**, *53*, 3780–3787. [CrossRef]

33. Kitamura, N.; Sakamoto, T.; Takebe, H. Effect of Reaction Layer on Water Durability in BaO–FeO–Fe2O3–P2O5 Glasses. *Mater. Trans.* **2018**, *59*, 437–442. [CrossRef]
34. Sun, J.; Liu, W.; Chang, W.; Zhang, Z.; Li, Z.; Yu, T.; Lu, M. Characteristics and formation mechanism of corrosion scales on low—Chromium x65 steels in CO_2 environment. *Acta Metall Sin* **2009**, *45*, 84–90.